AGU PUBLICATIONS

JGR

Journal of Geophysical Research: Atmospheres

RESEARCH ARTICLE
10.1002/2017JD026456

Key Points:
- Correction and extension of the MISR time series from March 2000 to February 2015 shows no significant trend in global cloud heights
- Southern Hemisphere cloud heights have risen, and Northern Hemisphere heights have fallen, especially in the extratropics
- Equatorial cloud heights show strong correlations in response to ENSO, up to 1.5 km interannual variations canceling zonally

Correspondence to:
R. Davies,
r.davies@auckland.ac.nz

Citation:
Davies, R., V. M. Jovanovic, and C. M. Moroney (2017), Cloud heights measured by MISR from 2000 to 2015, *J. Geophys. Res. Atmos.*, *122*, 3975–3986, doi:10.1002/2017JD026456.

Received 5 JAN 2017
Accepted 22 MAR 2017
Accepted article online 24 MAR 2017
Published online 7 APR 2017

Cloud heights measured by MISR from 2000 to 2015

Roger Davies[1], Veljko M. Jovanovic[2], and Catherine M. Moroney[2]

[1]Department of Physics, University of Auckland, Auckland, New Zealand, [2]Jet Propulsion Laboratory, California Institute of Technology, Pasadena, California, USA

Abstract Davies and Molloy (2012) reported a decrease in the global effective cloud height over the first 10 years of Multiangle Imaging Spectroradiometer (MISR) measurements on the Terra satellite. We have reexamined their time series for possible artefacts that might especially affect the initial portion of the record when the heights appeared anomalously high. While variations in sampling were shown to be inconsequential, an artefact due to the change in equator crossing time that affected the first 2 years was discovered, and this has now been corrected. That correction, together with the extension of the time series by five more years, yields no significant overall trend in global heights during the first 15 years of Terra operation. The time series is dominated by large interannual fluctuations associated with La Niña events that mask any overall trend on a global scale. On a regional basis, the cloud heights showed significant interannual variations of much larger amplitude, sometimes with fairly direct cancellation between regions. There were unexplained differences between the two hemispheres in the timing of height anomalies. These differences persisted over a large range of extratropical latitudes, suggestive of teleconnections. Within the tropics, there were very strong changes associated with the Central Pacific and Indonesian Maritime Continent regions that oscillated out of phase with each other, with interannual amplitudes that exceeded 1 km.

Plain Language Summary Effective cloud height is an important climate variable, strongly influencing the overall greenhouse effect, with a change of ≈15 m/decade being comparable to the rate of CO_2 increase. The Multiangle Imaging Spectroradiometer (MISR) instrument on the Terra satellite uses a stereo technique to systematically measure cloud heights with a sampling accuracy of ≈11 m on the global, annual average. Over the last 15 years we find interannual departures are greatest during La Niña events, reaching over 40 m on a global average. The apparent decreasing trend during the first 10 years noted by Davies and Molloy has now vanished, in part due to correction for sun glint, and in part due to higher clouds in the last 5 years. Regional cloud height changes continue to show a high degree of correlation, especially for about five distinct regions of equatorial clouds. Southern Hemisphere cloud heights have increased, whereas Northern Hemisphere heights have decreased.

1. Introduction

The effective height of clouds, H, is defined [*Davies and Molloy*, 2012, DM12 hereafter] as the height-weighted probability of occurrence, $f(h)$, of a cloud-top or cloud-free surface of height h. That is, $H = \int_0^\infty hf(h)\mathrm{d}h$. In this paper we distinguish between H_G, the global value, and H_R, the value pertaining to some defined region R. H_G is one of the most important controls of the Earth's climate system, consistent with the theory of radiative-convective equilibrium [*Manabe and Strickler*, 1964; *Popke et al.*, 2013]. For a planet in radiative equilibrium, the amount of outgoing longwave radiation must equal the absorbed shortwave radiation, regardless of H_G. The effective temperature from which the emission to space occurs is thus fixed [for given insolation and albedo]. Below H_G the transfer of energy is mainly by convection, so that the higher the value of H_G, the higher must be the surface temperature [for fixed lapse rate]. The complete theory includes the effective height of spectrally active gases above grey emission from clouds and the surface, but if we focus only on *changes* in H_G, there is a simpler model of planetary climate that tells us [*Schneider*, 1972]: as surface temperatures rise, a sustained decrease in H_G would imply a negative feedback mechanism, slowing the rate of change of temperature, and vice versa.

To put this in context, the current increase in CO_2 of 5–6% decade^{-1} would increase equilibrium surface temperature by ≈ 90 mK/decade *in the absence of other feedback mechanisms*. A modern radiative-convective

equilibrium model [*Davies and Radley*, 2009] shows that a similar change in equilibrium surface temperature would result from an increase in H_G of ≈ 15 m/decade, again *in the absence of other feedbacks*. As discussed later in this paper, the annual sampling error in H_G using Multiangle Imaging Spectroradiometer (MISR) measurements is ≈ 11 m. This allows us to distinguish between positive and negative linear trends in H_G, should they exist, greater than ≈ 7 m/decade with a 15 year time series.

As noted in DM12, changes in H_R can be much larger than changes in H_G, depending on the region. These changes are usually associated with changes in horizontal transport and are also correlated over broad regions, yielding useful observations of global teleconnections related to changes in other variables, especially the Southern Oscillation Index, or more generally to the Hadley-Walker circulations. Since the global changes must be the net of all regional changes, a complete understanding of the longwave effect of clouds on surface temperature, especially the nature of cloud feedback, goes beyond the simple radiative-convective perspective and involves far more than just geometric height. Changes in cloud emissivity, lapse rate, and circulation patterns (especially affecting vertical motion), to name a few, must all be considered. In this paper, however, we focus on the overall 15 year time series of H_R and defer the episodic relationship between geometric heights and other variables during El Niño or La Niña events to a subsequent study.

Absolute values of H depend critically on the technique being used and cannot generally be directly compared. Differential changes in H, on the other hand, may be comparable between different measurement techniques and between measurements and models, provided the respective time series are internally consistent. As a cautionary note, H is defined geometrically and is best measured by techniques that are independent of the temperature profile, such as by MISR [*Moroney et al*., 2002] and CALIOP [*Winker et al*., 2009]. Alternate approaches by observations or models that obtain cloud heights based on pressure or temperature will necessarily also be affected by any changes in the temperature profile.

DM12 presented observational results from the MISR instrument on the Terra satellite from March 2000 to February 2010. The linear trend in H_G was -44 ± 22 m/decade. However, this was influenced in part by high values at the start of the record, prompting *Evan and Norris* [2012, EN12 hereafter] to hypothesize that the DM12 results are a consequence of fewer measurements at the start of the time series, supposed by EN12 to be due to coregistration issues that might depend on scene type. EN12 noted a correlation between total measurement counts and the relative distribution of counts into different height bins. They interpreted this correlation as potentially creating a high bias of the effective heights measured in the first two years of the decade compared with those based on greater sampling throughout the remainder of the decade. EN12 speculated that if this apparent bias were to be removed, the effective height might have risen, rather than fallen, over the first decade of MISR measurements. We have subjected the data to a rigorous reanalysis and have made a number of improvements as described below. Most of these had a minor effect, and we found no issues due to the initial reduced sampling. We did, however, discover one significant artefact. This was due to the shift in the position of sun-glint that occurred during the first 2 years, and we describe how we have now corrected for this. With five additional years of data now available, we also extend the time series out to a decade and a half. We summarize our findings for both H_G and H_R, choosing regions that address hemispheric asymmetry, differences between the tropics and extratropics, and differences within the tropics.

2. Revised Data Analysis

While much of the data analysis was similar to DM12, we have made a number of minor changes, and one major change, that improve the consistency of the time series.

2.1. Restricted Global Coverage

To obtain H_G, DM12 included polar data all the way to the terminator. With orbital fluctuations, the highest latitudes sampled in a given month can vary slightly from year to year. To provide uniform sampling throughout the entire time series, we have now restricted the "global" integral of heights to 90% of the Earth's surface area, omitting all data north of 71.8°N and south of 71.8°S. This had a minor effect on the overall changes in H_G.

2.2. Change From 2.2 km to 1.1 km Resolution

The MISR produces stereo-derived heights at 1.1 km resolution that are used to generate a Reflecting Layer Reference Altitudes (RLRA) at 2.2 km resolution that are later used to determine local albedos. When the

1.1 km data vary in the 2 × 2 array, the RLRA is based on the highest value to minimize obscuration effects. Consequently, the absolute value of H_G at 1.1 km is lower than that at 2.2 km by about 300 m. While the height anomalies are very similar, the 1.1 km heights proved more useful in the sun-glint correction described below, so these are now used instead of the RLRAs.

2.3. Change in Temporal Binning

DM12 binned data into approximate 10 day intervals by month. The Terra satellite, however, has a 16 day repeat cycle in terms of its 233 distinct orbital paths. To provide the most uniform grouping of paths per time bin, minimizing path-aliasing and the end-of-year remnant, the time bin was changed to 14 consecutive days (about 204 paths per bin), rather than by month, giving 26 groups per year. Consistent with the sampling changes described next, this made no appreciable difference to the DM12 results.

2.4. Uniform Sampling: By Counts and Paths

One potential artefact in the original analysis, as mentioned by EN12, might be attributable to the reduced number of samples in the first 2 years compared with the rest of the time series. To address the issues raised by EN12, we note that there are two relevant data sets. One is the MISR Level 3 cloud-height product (CGCL version 24) that was used by EN12. This provides monthly counts in 15 height bins from 0 to 19 km, together with the mean height within each height bin. These are on a 0.5° lat-lon grid and represent a conveniently compact data set, usable for many applications. The other data set, as used by DM12, is based on the MISR Level 2 cloud-height product (TC_STEREO version 17) and summarizes the distributions of cloud height in more detail at the block level, orbit by orbit. [A slightly different Level 2 data product, TC_CLOUD, was also examined, but it produced very similar anomalies to TC_STEREO for most of the time series, with only subtle differences, apparently due to the detection of high cirrus, and is not discussed further here.] A "block" contains overlap data between MISR's 9 cameras, measuring 140 km along-track and 380 km across-track. The main difference between the two data sets of relevance to this paper is the ability to directly examine the effect of sampling frequency using Level 2 data that is not possible using Level 3 data. Both data sets refer to "without-wind" heights (that is, stereoscopically derived heights that have not been corrected for advection due to the along-track component of the wind vector). For reasons explained in DM12, the "without-wind" data are independent of wind calculations needed for the "best-wind" product to correct for advection and have the best coverage.

EN12 defined the total global counts, c_t, as the globally averaged number of observations going into each 0.5° lat-lon grid element per month at Level 3, suitably weighted by area. The time series of c_t from the start of MISR data collection in March 2000, through February 2011, is shown in Figure 1a (adapted from EN12 Figure 1b). There were generally fewer counts in the first 26 months than in most of the rest of the time series. The number of orbits per month as used by Level 3 is also shown in Figure 1a. It is clear that the main reason for variation in counts per month is the variation in the number of orbits per month available for Level 3 processing.

Turning to the orbit availability, Figure 1b shows the total number of orbits per month for which MISR was turned on in a data-collecting mode. These average about 428 orbits/month, but there are occasional dropouts, so that the median count is higher, at 434 orbits/month. The high frequency ripple noted throughout much of the time series is due to month boundaries and to the different month lengths.

However, not every orbit is completely usable for MISR stereo retrievals, for two separate reasons. The first of these has to do with the quality of navigation and attitude information provided by the Terra spacecraft. Data files provided to the science data processing teams contain quality flags associated with conditions such as limit violations, data gaps, etc., that alert the teams to potential issues with the accuracy of the spacecraft navigation and attitude [*Raytheon*, 2004]. Whenever these flags affect a nontrivial segment of the data, the entire orbit is excluded from the stereo processing and these data do not reach Level 3. These orbits were also excluded by DM12 in their analysis. Excluded orbits were more prevalent early in the mission, mainly due to more frequent satellite maneuvering events. Neither scene type nor stereo processing influences these excluded orbits, because they are due entirely to spacecraft operations. If the excluded orbits occurred randomly within any given month, there would be no reason to expect any effect on the monthly height anomalies other than increased variance due to fewer samples. Figure 1b shows the number of orbits per month affected by this. The median count is about six orbits per month, but over 100 orbits/month were affected at times early in the mission.

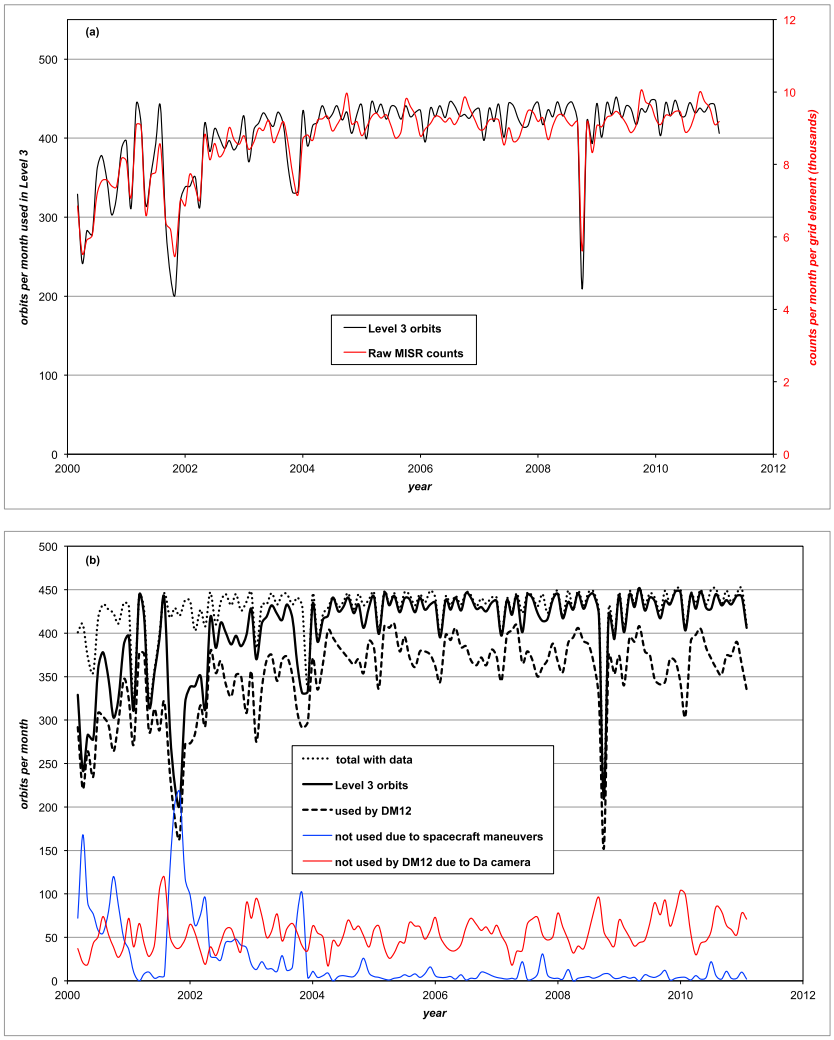

Figure 1. (a) Orbits per month used in Level 3 (black, left axis) and raw MISR counts per month per 0.5° grid element adapted from EN12 (red, right axis). (b) Orbits per month: total orbits with data (black, dotted); orbits used by EN12 in Level 3 (black, solid); orbits used by DM12 (black, dashed); orbits unusable due to Terra maneuvers not used by Level 3 or DM12 (blue); orbits with poor Da registration not used by DM12 (red).

For a different reason, some orbits that are not flagged as suspect by the spacecraft operations may also be excluded from subsequent parts of the stereo processing. This is the only "coregistration problem" alluded to by EN12. As discussed by *Jovanovic et al*. [2007], additional processing steps have been implemented to deal with an intermittent problem that affects the coregistration of the Da camera. This camera has a backward-looking oblique view angle of 70.5° and must be coregistered to the backward-looking Ba (45°) camera as part of the MISR stereo wind retrieval. As a part of the quality checks during the stereo processing, some of the orbits are conservatively flagged as suspect in regards to coregistration and ignored by the wind-processing algorithm. In any event, the without-wind stereo heights use only the three near-nadir cameras, so this flag is ignored in processing the Level 3 without-wind heights. In their analysis of Level 2 without-wind heights, DM12 observed this flag with, in hindsight, unnecessary caution. This coregistration issue affects a median number of 53 orbits/month. Unlike the spacecraft maneuvering issue, the number of orbits/month with suspect Da coregistration has been relatively constant throughout the mission. More importantly, the quality of the imagery from any of the oblique cameras (including Da) has no impact on the accuracy of the without-wind heights.

Figure 1b summarizes how these different factors affect the number of orbits processed per month. The Level 3 orbit counts are affected only by the spacecraft maneuvers and consequently closely match the total

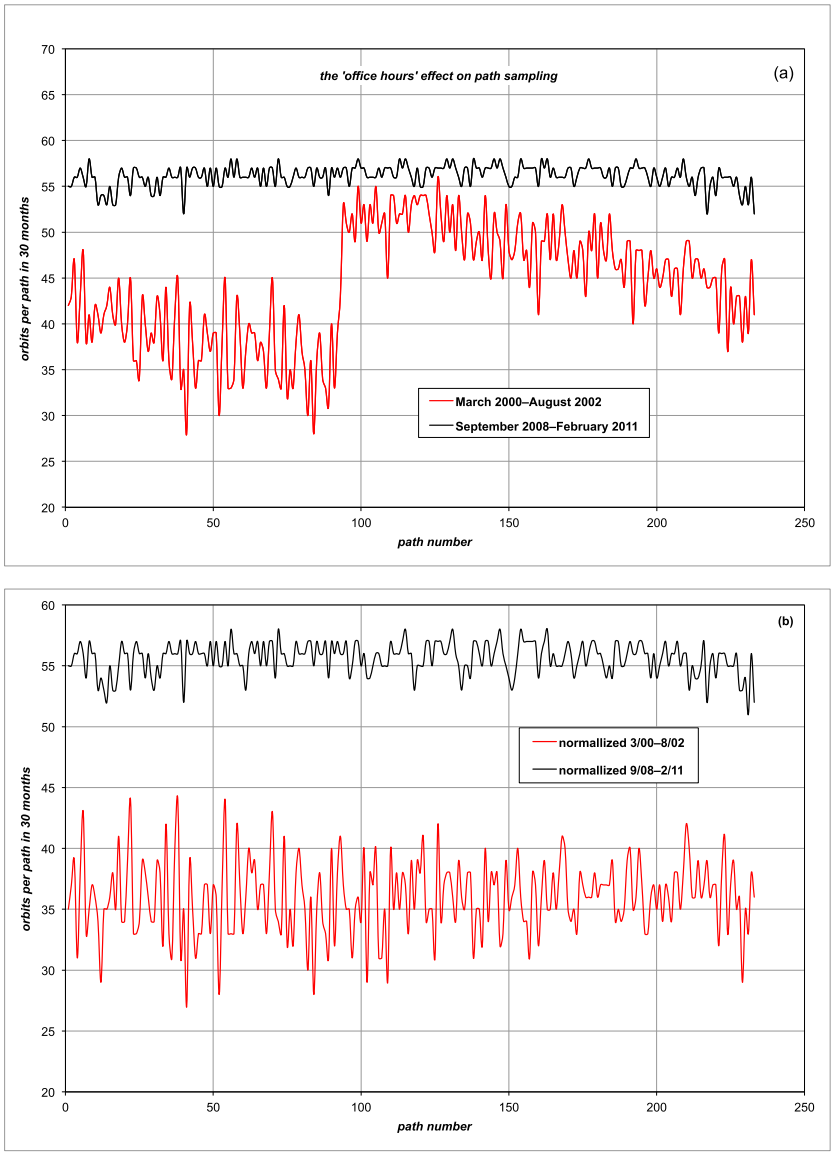

Figure 2. (a) Orbits with valid data in a 30 month period, by path number. First 30 months, 3/2000–8/2002 (red), typical 30 months 9/2008–2/2011 (black). (b) Same as Figure 2a, but after random omission of orbits to yield uniform sampling.

number of orbits with data for most of the time series after the first 2 years. The orbits analyzed by DM12 show very similar time dependence, but because DM12 conservatively omitted the orbits affected by the coregistration issue, they are offset from Level 3 by roughly 53 fewer orbits/month.

Deeper analysis of the reduction in data volume during the earliest part of the mission revealed an unexpected finding. The Terra satellite follows a sequence of 233 unique orbital paths that are repeated every 16 days. These are numbered from east to west, with adjacent paths separated by about 1.5° at the equator. For example, path 1 crosses the equator at about 65°W and path 95 crosses at about 150°E. When sampling is stratified by path number over a 30 month period, the first 30 months have nonuniform sampling compared to subsequent 30 month intervals, as shown in Figure 2a. The reduction in sampling caused by spacecraft maneuvers is clearly not random by path. The reason appears to be attributable to the normal working hours of the Terra operations team at the NASA Goddard Space Flight Center. The discontinuity in sampling density at path 94 occurs at about 4 P.M. Eastern time in the USA.

To investigate whether any actual bias was introduced by this "office hours" effect, we applied an alternative form of sampling on a monthly basis. Because there can be at most only two orbits per path per month,

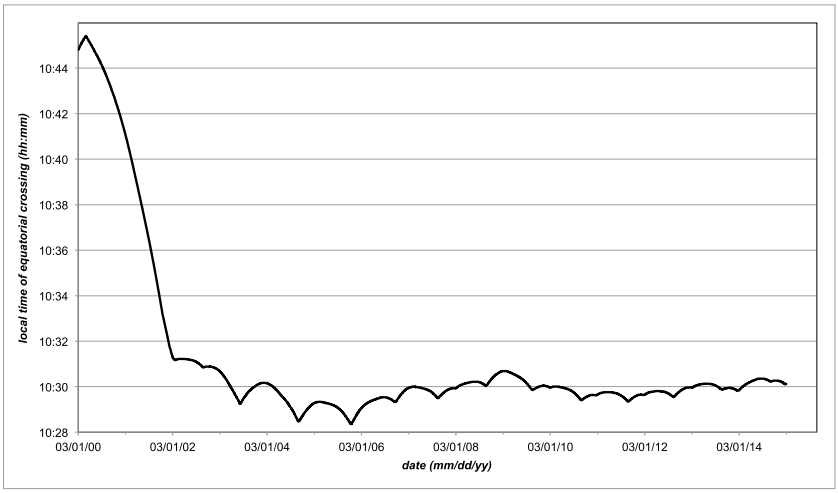

Figure 3. Mean local time of daytime equator crossing of the Terra satellite.

adjacent paths were grouped into six groups of about 39 paths each, and the total orbits per group noted. For any given month, orbits were randomly removed from more populated groups to match the population of the least populated group. This reduced the average sampling in the first 30 months to about 280 orbits/month, but now uniformly by path number, as shown in Figure 2b. The height anomalies were analyzed as before, and while the anomalies for some months changed slightly, the effects appeared to be random and the overall trend remained well within the estimated uncertainty. Despite the sharp discontinuity in path sampling, this had little effect on the overall results. The reduced sampling in the early part of the mission simply increased the variance slightly and had no effect on the trend analysis.

To avoid any risk of future path sampling biases, the calculation of anomalies was changed from being dependent on large groups of paths to being calculated path by path.

2.5. Uniform Sampling: By Glitter Angle

The Terra satellite is in a sun-synchronous orbit, with a nominal 10:30 A.M. equator crossing time (descending). At the start of the mission, this crossing time was about 10:45 A.M. The crossing time changed systematically for about 2 years until it stabilized at a value of about 10:30 A.M., where it has remained since, as shown in Figure 3. From a meteorological perspective, not much happens to cloud heights in 15 min in the midmorning, especially to the upper level cloud heights that contribute the most to the effective-height signal. However, from a remote sensing perspective, there is a change in the illumination conditions that affect the detectability of high clouds. We find that more high clouds are detected in the presence of sun-glint, presumably due to enhanced contrast that detects thinner clouds over the ocean. The change in detection is due to the shift in the location of the subsun point by about 4° in longitude over 15 min. Because of this, there was more sun-glint at the eastern edge of the blocks at some latitudes at the beginning of the mission compared to no change over the rest of the mission. This affected the relative sampling of data as a function of glitter angle, which is the angle between the viewing direction and the direction of specular reflection from the Sun [*Bull et al.*, 2011]. A glitter angle of 0° looks directly at the sun-glint. By examining the glitter angle for the An camera for each sample number across-track [these range from 1 to 512 at 1.1 km resolution, from left to right across-track, but the first and last ≈ 50 sample numbers are not used due to lack of overlap with the other stereo cameras] at the start of the mission, compared with the stable situation, taking 2005 as a reference, it was possible to reverse engineer the effect of orbital change on glitter angle by identifying a common set of glitter angles for each block and Julian day of year. For example, Figure 4 shows the glitter angles by sample number for one of the worst situations, comparing those in 2000 with those in 2005. Here the subset of glitter angles that is common to both years makes up about 87% of the usual sample space. The revised analysis therefore first provided a map of sample numbers by block and day for each year that shared identical glitter angles. Cloud heights from only these sample numbers were used in the revised analysis, ensuring uniform sampling by glitter angle across the entire time series. This

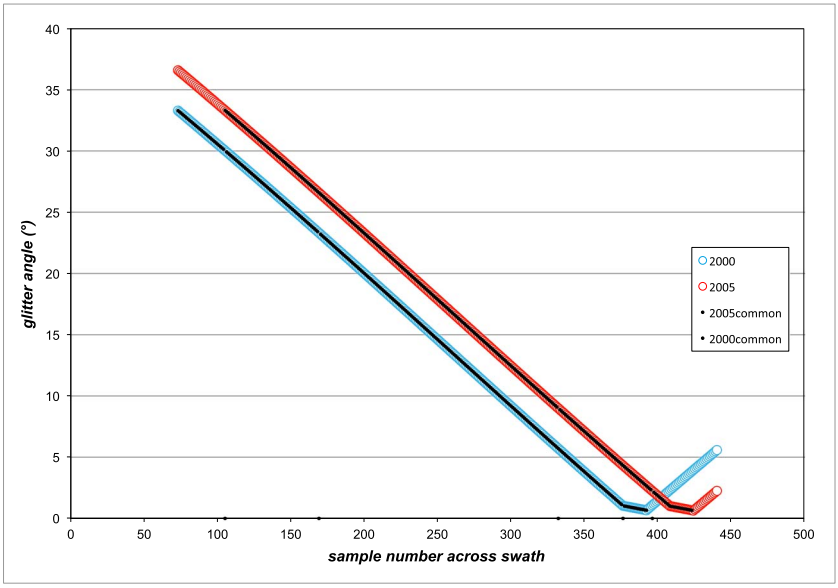

Figure 4. Example of glitter angles as a function of cross-track position (sample number), for 23°N, mid-March 2000 (blue) and 2005 (red). The black points show common sampling of glitter angles for the 2 years.

had a significant effect on the height anomalies in the first 2 years, as noted in the next section, and turned out to be far more significant than the revisions discussed in sections 2.1 to 2.4.

3. Time Series of Global Effective Height Anomalies, H'_G

Height anomalies were calculated in the same manner as DM12, but with the changes noted above. The baseline average $\langle H_G \rangle$ was taken from March 2002 to February 2015, in 14 day increments, path by path, and the anomalies $H'_G = H_G - \langle H_G \rangle$ were averaged over all paths and smoothed using a 1 year running mean. The time series shown in Figure 5 spans 15 complete years, from March 2000 to February 2015. It is similar to Figure 1 of DM12 but has been extended by an additional 5 years and is now based on the 1.1 km Stereo height without-wind product from Level 2 of the MISR data product [*Bull et al.*, 2011]. Note the significant change from DM12 in the height anomalies during the first 2 years due to the shifting of the glitter pattern. Heights over the last 5 years have also been higher than the previous average. The combination of reduced

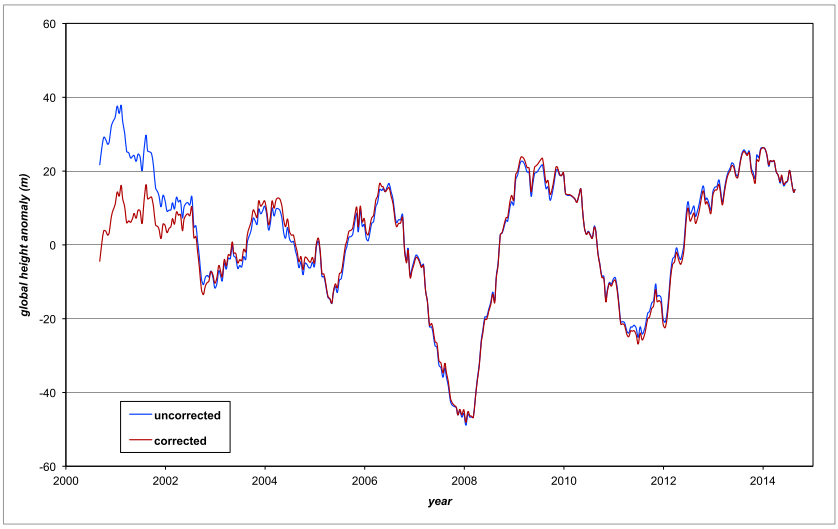

Figure 5. The 15-year time series of global height anomalies from March 2000 to February 2015. Corrected for shift in glitter pattern (brown), and uncorrected (blue). Data have been smoothed by a 12 month running mean.

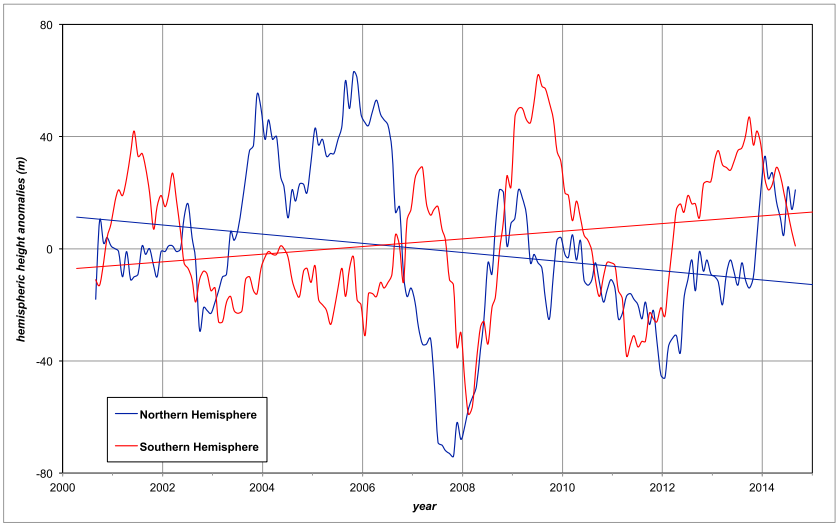

Figure 6. Hemispheric height anomalies from March 2000 to February 2015. Northern Hemisphere (blue) decreased at −16 ± 5 m/decade. Southern Hemisphere (red) increased at 14 ± 4 m/decade.

heights at the beginning of the record due to the glint correction and the above-average heights over the last 5 years causes the negative trend noted by DM12 to vanish, and any overall change in height is statistically insignificant. We do not see an overall increase in global height, as noted by *Norris et al*. [2016], but their analysis spanned a different time period and did not use geometric cloud heights.

There is a small sampling error in the annual mean anomaly due to the sparse coverage of MISR measurements. From earlier studies by *Cahalan et al*. [1982] and *Davies* [1994], we know that the spatial coherence of cloud fluctuations is less than ≈ 1000 km and the temporal coherence is less than ≈ 2 days. The narrow cross-track swath width of MISR (≈380 km) provides complete spatial independence from one orbit to the next [consecutive orbits are separated by ≈ 2500 km at the equator], and even at high latitudes, where it is shortest, the repeat coverage is 2 days, stretching to 9 days at low latitudes. Each orbital average thus represents an independent sample of $H_G^{'}$. The standard deviation of single orbit values of $H_G^{'}$ is ≈ 780 m, resulting in an expected sampling error of the annual mean $H_G^{'}$ of ≈ 11 m [≈5100 orbits typically]. Interannual variations in $H_G^{'}$ that are significantly greater than this sampling error should therefore be Earth system related.

The main features of interest are the sudden ephemeral decreases in effective height 2007–2008 and 2011, loosely associated with La Niñas, and the high values in 2009 and since 2013, loosely associated with El Niños.

4. Time Series of Regional Effective Height Anomalies, $H_R^{'}$

The time series of global height anomalies masks several competing effects that are more evident when the data are viewed regionally. While this is a rich data set that deserves more analysis, here we address only broad regional influences.

Figure 6 shows the time series separately for the Northern and Southern Hemispheres, again excluding data poleward of 71.8°. These data have been corrected for changes in sun-glint and are uniformly sampled by path. The Northern Hemisphere height anomalies show a slight decrease [−16 ± 5 m/decade. Note that in this and the following, the trends are simply the best-fit linear trend, with the uncertainty that of the regression fit.], compensated by a slight rise in the Southern Hemisphere [+14 ± 4 m/decade]. Both hemispheres responded to the 2008 La Niña, with the Northern Hemisphere reacting about 6 months prior to the Southern Hemisphere. Otherwise, the height anomalies in the respective hemispheres appear to be uncorrelated [$r = 0.02$]. When stratified further into a three-band planet, composed of the tropics (30°S–30°N) and the northern and southern extratropics (30°–71.8°), as shown in Figure 7, the northern extratropics heights have fallen [−29 ± 7 m/decade] and the southern extratropics heights have risen [+22 ± 5 m/decade]. The tropics overall show no apparent trend in effective height. This stratification is roughly consistent with Figure 6, except that the southern extratropics have an initial year of strongly negative anomalies, whereas the

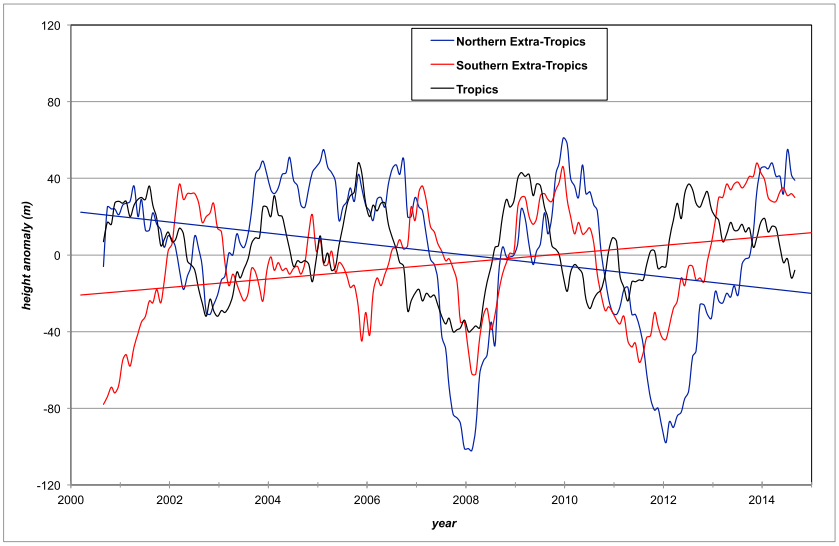

Figure 7. Height anomalies from March 2000 to February 2015 for tropical, 30°S–30°N (black), northern extratropics, 30°N–72°N (blue), and southern extratropics, 30°S–72°S (red). Tropics shows no significant trend, northern extratropics decreased at -29 ± 7 m/decade, and southern extratropics increased at 22 ± 5 m/decade.

whole Southern Hemisphere had positive anomalies then. The southern extratropical anomalies show no overall correlation [$r = -0.02$] with the tropics, whereas the northern extratropical anomalies have a correlation coefficient of $r = 0.28$ with the tropical anomalies. Unlike the hemispheric values, the northern and southern extratropical anomalies are correlated, with $r = 0.35$.

The presentation of tropical anomalies in Figure 7, however, disguises major changes that occur longitudinally. As was shown earlier by DM12, there is a region in the Central Pacific [roughly bounded by 2.9°S–2.9°N,

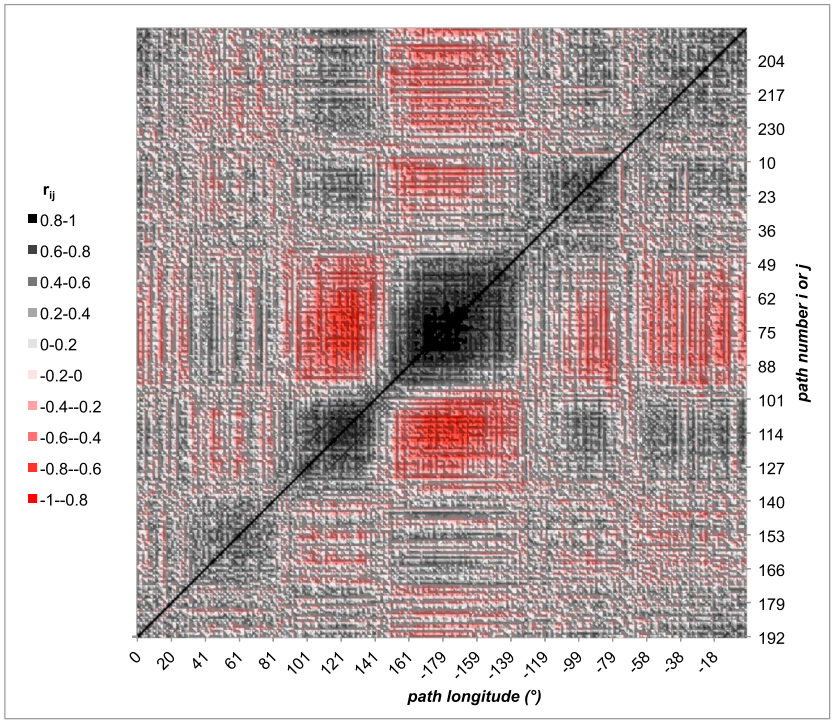

Figure 8. Correlations, r_{ij}, between paths i and j, in the equatorial height anomalies [1.9°S–1.9°N] from March 2000 to February 2015. i and j range from 1 to 233, mapping to longitudes as shown on the x axis.

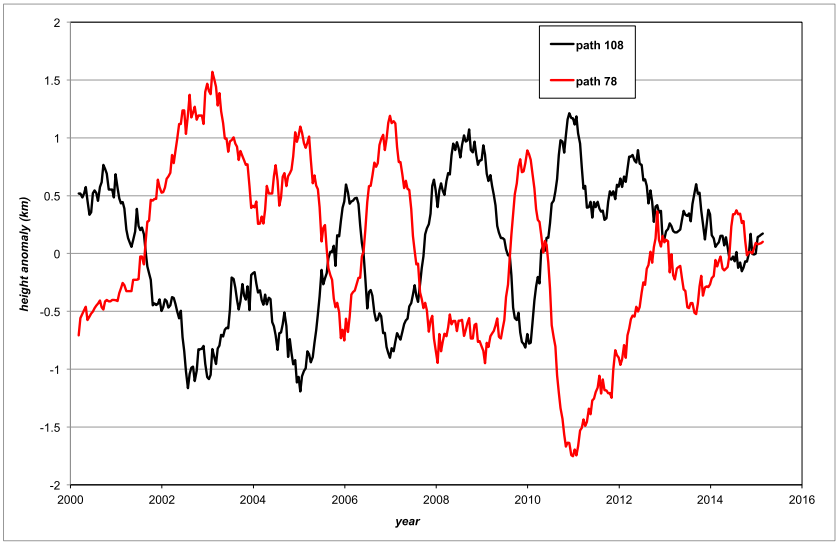

Figure 9. Equatorial height anomalies from March 2000 to February 2015, for paths 78 (red) and108 (black), with equatorial longitudes 176°E and 130°E, respectively. $r_{78,108} = -0.91$.

160°E–160°W] that oscillates out of phase with a region in the Maritime Continent [roughly bounded by 2.9°S–2.9°N, 104°E–133°E]. To examine this further, we calculated the path-path correlation coefficients between all paths, for their respective height anomalies over the 15 year time series. While there are significant correlations between path groups over a global range of latitudes, the strongest results occur for equatorial latitudes between about 2°S and 2°N, or 10% of the Earth's surface. These correlations are shown in detail in Figure 8, which is based on the path-path correlations between all paths, in the latitude range 1.91°S to 1.91°N. That is, we show the values of r_{ij} for all $i, j \in [1, 233]$, where r_{ij} is the cross-correlation coefficient of height anomalies for paths i and j over the 15 year time series, limited to this latitude range. Clearly, $r_{ij} \equiv 1$ for $i = j$ [the black diagonal line], and $r_{ij} \equiv r_{ji}$. While the analysis is done using path numbers, the corresponding longitudes are also shown on the figure [positive for East, and negative for West. That is, 0° corresponds to i or $j = 192$, 180° to i or $j = 76$, and so on]. We note the following main features.

1. The correlation coefficients appear grouped into positive values over about five distinct equatorial regions, of which the Central Pacific [160°E to 150°W, paths 56–88] is the largest, followed by the Maritime Continent [105°E to 138°E, paths 103–124]. The others are centered on 94°W (Eastern Pacific), 58°E (West Indian Ocean), and 11°W (East Atlantic).
2. The Central Pacific and Maritime Continent are negatively correlated, with the strongest anticorrelation $r_{78,108} = -0.91$ occurring between paths 78 and 108 [176°E and 130°E]. The time series of these two paths is shown in Figure 9. Separated by about 4600 km, cloud height anomalies of these paths are nonetheless very closely related. Interannual deviations of ≈ 1.5 km in the Central Pacific path are approximately concurrent with ≈ 1 km opposite deviations in the Maritime Continent path.
3. Widely separated regions can be positively correlated. The strongest example is between the Maritime Continent and East Atlantic, paths 112 and 201, respectively, with $r_{112,201} = 0.75$. The corresponding time series are shown in Figure 10. Interannual deviations in cloud heights of up to 1 km can be in phase, particularly from 2008 through 2010.

5. Summary

5.1. On the Uniformity of the Time Series

By correcting for an artefact caused by a shift in local mean equatorial crossing time during the first 2 years that affected the detection of high clouds in the vicinity of sun-glint, we have improved the quality of MISR's time series of cloud height anomalies. We examined several other sampling issues but found none of these to be significant. Due to more frequent spacecraft maneuvers, fewer orbits in the first 30 months had fully registered data and we discovered that the resultant sampling by path number was not completely

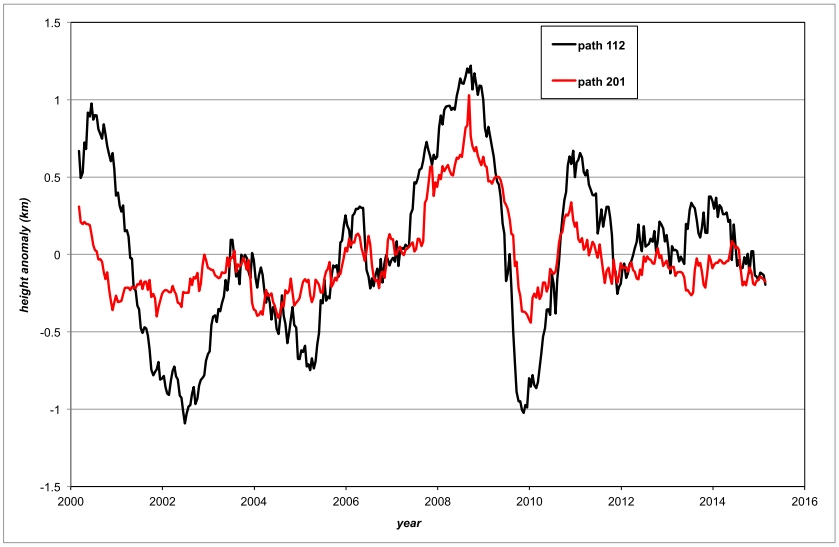

Figure 10. Equatorial height anomalies from March 2000 to February 2015, for paths 112 (black) and 201 (red), with equatorial longitudes 124°E and 14°W, respectively. $r_{112,201} = 0.75$.

uniform [an "office hours" effect]. Fortunately, this type of nonuniform sampling was shown [by randomly removing orbits elsewhere to restore uniformity] to have had no significant effect on the overall results.

EN12 speculated that the correlation between global counts and effective height [through the relative counts in different height bins] was due to frequency of sampling. By randomly removing orbits from the subsequent time series to match the initial sampling frequency, we found no such effect. The correlation arose because heights appeared higher at the start of the mission when there were coincidentally fewer data. The minor data loss due to the Da camera coregistration discussed in EN12 does not affect the without-wind height product used in DM12, EN12, and here.

Correction of the sun-glint artefact and tests of the "office hours" effect and sampling frequency necessarily requires use of the Level 2 stereo height data at the block or pixel level. On the other hand, since the data continue to be very uniformly sampled and processed after the first two years [as long as the current equator crossing time can be maintained], the present version of Level 3 data summaries should be quite useful from 2003 onwards.

5.2. On the Global Time Series Results

Correction of the sun-glint artefact reduced the early height anomalies noted by DM12. Together with the addition of five more years when global heights have been higher than the average over the first 10 years, the overall trend in the global effective heights over 15 years now appears to be insignificant [Figure 5]. The most interesting global features are the strong excursions in the global mean effective height loosely associated with La Niñas [2007–2008 and 2011] and El Niños [2009, 2013ff]. Since these tend to dominate the time series, a much longer series will be needed before we can resolve the question as to whether there is a net positive or negative feedback of global effective cloud height in response to global warming.

The MISR approach to measuring geometric cloud heights from stereo pattern matching still appears to be the best bet for obtaining such a time series. The data from CALIOP are more precise locally but have a larger sampling error for the global mean. The ISCCP approach [*Norris et al.*, 2016] covers a longer time period but is not sufficiently uniform and is also dependent on temperature profiling for its interpretation.

5.3. On the Regional Time Series Results

Turning from global to regional trends, we note that the two hemispheres have behaved differently over the last 15 years. Northern Hemisphere effective heights have decreased, and Southern Hemisphere heights have increased, both at the rate of about 10 m/decade [Figure 6]. These rates increase to between 20 and 30 m/decade when the tropics are excluded.

Even though the tropics as a whole showed no significant trend, this is where the strongest regional interannual variations were observed. Two key regions are centered on the equator at longitudes of about 122°E and 175°W, each of area greater than 10^6 km^2. Their heights fluctuate out of phase with each other in response to La Niñas or El Niños, with annual mean amplitudes that can exceed 1 km. Elsewhere around the equatorial band, there are three other broad regions that show a weaker, but still clearly statistically related, evidence of teleconnections that affect cloud heights.

The strong positive and negative departures in regional cloud heights, attributed to La Niñas and El Niños, currently mask any overall cloud trend in global cloud height. The temporal propagation of regional variations in cloud height during a strong El Niño or La Niña may provide useful information on global teleconnections, and this seems worthy of more intensive future analysis.

Acknowledgments
We thank the MISR group, especially D. J. Diner and K. J. Mueller, for helpful discussions. This research was supported by subcontract 1460339 between the California Institute of Technology/Jet Propulsion Laboratory and The University of Auckland. The original data sets were obtained from the NASA Langley Research Center Atmospheric Science Data Center, eosweb.larc.nasa.gov. All derived data are available directly from the figures. The equator crossing times were provided by the EOS Flight Dynamics Team, NASA Goddard Space Flight Center. The authors thank three anonymous reviewers for comments that have improved this paper.

References

Bull, M., J. Matthews, D. McDonald, A. Menzies, C. Moroney, K. Mueller, S. Paradise and M. Smyth (2011), MISR Data Product Specifications, Jet Propulsion Laboratory D-13963, Revision S. [Available at https://eosweb.larc.nasa.gov/project/misr/dps.]

Cahalan, R. F., D. A. Short, and G. R. North (1982), Cloud fluctuation statistics, *Mon. Weather Rev.*, *110*, 26–43, doi:10.1175/1520-0493(1982)110<0026:CFS>2.0.CO;2.

Davies, R. (1994), Spatial autocorrelation of radiation measured by the Earth Radiation Budget Experiment: Scene inhomogeneity and reciprocity violation, *J. Geophys. Res.*, *99*, 20,879–20,887, doi:10.1029/94JD01680.

Davies, R., and C. Radley (2009), Radiative-convective equilibrium revisited: The greenhouse effect of clouds, in *Current Problems in Atmospheric Radiation (IRS 2008)*, *AIP Conf. Proc.*, vol. 1100, edited by T. Nakajima and M. A. Yamasoe, pp. 667–670, doi:10.1063/1.3134603.

Davies, R., and M. Molloy (2012), Global cloud height fluctuations measured by MISR on Terra from 2000 to 2010, *Geophys. Res. Lett.*, *39*, L03701, doi:10.1029/2011GL050506.

Evan, A. T., and J. R. Norris (2012), On global changes in effective cloud height, *Geophys. Res. Lett.*, *39*, L19710, doi:10.1029/2012GL053171.

Jovanovic, V., C. Moroney, and D. Nelson (2007), Multi-angle geometric processing for 3 globally geo-located and co-registered MISR image data, *Remote Sens. Environ.*, *107*, 22–32, doi:10.1016/j.rse.2006.08.013.

Manabe, S., and R. F. Strickler (1964), Thermal equilibrium of the atmosphere with a convective adjustment, *J. Atmos. Sci.*, *21*, 361–385.

Moroney, C., R. Davies, and J.-P. Muller (2002), Operational retrieval of cloud-top heights using MISR data, *IEEE Trans. Geosci. Remote Sens.*, *40*, 1532–1540.

Norris, J. R., R. J. Allen, A. T. Evan, M. D. Zelinka, C. W. O'Dell, and S. A. Klein (2016), Evidence for climate change in the satellite cloud record, *Nature*, *536*, 72–75.

Popke, D., B. Stevens, and A. Voigt (2013), Climate and climate change in a radiative-convective equilibrium version of ECHAM6, *J. Adv. Model. Earth Syst.*, *5*, 1–14, doi:10.1029/2012MS000191.

Schneider, S. H. (1972), Cloudiness as a global climatic feedback mechanism: The effects on the radiation balance and surface temperature of variations in cloudiness, *J. Atmos. Sci.*, *29*, 1413–1422.

Raytheon Systems Company (2004), Terra Spacecraft Ephemeris and Attitude Data Processing, 500-EMD-001, Revision 1.

Winker, D. M., M. A. Vaughan, A. Omar, Y. Hu, K. A. Powell, Z. Liu, W. H. Hunt, and S. A. Young (2009), Overview of the CALIPSO mission and CALIOP data processing algorithms, *J. Atmos. Oceanic Technol.*, *26*, 2310–2323, doi:10.1175/2009JTECHA1281.1.